Polar Jet Associated Circulation Triggered a Saharan Cyclone and Derived the Poleward Transport of the African Dust Generated by the Cyclone

Diana Francis, Clare Eayrs, Jean-pierre Chaboureau, Thomas Mote, David Holland

Journal of Geophysical Research: Atmospheres

RESEARCH ARTICLE
10.1029/2018JD029095

Key Points:
- A meandering polar jet initiated cyclogenesis over North Africa which caused a big dust storm in April 2011
- The meandering polar jet favored the transport of the uplifted dust toward the Arctic through cut-off low formation
- Ice melt occurred over southeastern Greenland during this event

Correspondence to:
D. Francis,
diana.francis@nyu.edu

Citation:
Francis, D., Eayrs, C., Chaboureau, J.-P., Mote, T., & Holland, D. M. (2018). Polar jet associated circulation triggered a Saharan cyclone and derived the poleward transport of the African dust generated by the cyclone. *Journal of Geophysical Research: Atmospheres*, *123*. https://doi.org/10.1029/2018JD029095

Received 1 JUN 2018
Accepted 30 SEP 2018
Accepted article online 10 OCT 2018

Polar Jet Associated Circulation Triggered a Saharan Cyclone and Derived the Poleward Transport of the African Dust Generated by the Cyclone

Diana Francis[1], Clare Eayrs[1], Jean-Pierre Chaboureau[2], Thomas Mote[3], and David M. Holland[1,4]

[1]NYUAD Institute, New York University Abu Dhabi, United Arab Emirates, [2]Laboratoire d'Aérologie, Université de Toulouse, CNRS, UPS, Toulouse, France, [3]Department of Geography, University of Georgia, Athens, Georgia, USA, [4]Center for Atmosphere Ocean Science, Courant Institute of Mathematical Sciences, New York University, USA

Abstract In this study, we identify a new mechanism by which dust aerosols travel over long distances across the eastern side of the North Atlantic Ocean toward the Arctic. The meandering polar jet was at the origin of both dust emission through cyclogenesis over Northwest Africa and poleward transport of the uplifted dust toward the Arctic, through cut-off circulation. The dust emission was associated with an intense Saharan cyclone that formed over Northwest Africa in early April 2011. The formation of the cyclone was caused by the intrusion into subtropics, of a high-latitude-upper-level trough, linked to the meandering polar jet. The trough initiated cyclogenesis over Northwest Africa after orographic blocking by the Anti-Atlas Mountains. The still meandering polar jet led to the formation of a cut-off low further south with which the Saharan dust-cyclone merged 2 days later and moved northward with the main stream. Beside satellite observations, a simulation at high resolution was performed using the prognostic-dust permitting model MesoNH. The total dust load carried during this event to areas located north of 40 N was estimated by the model to be 38 Tg and dust deposition was estimated to be 1.3 Tg. The Saharan dust reaching Greenland was accompanied by warm and moist air masses that caused a rise in surface temperature of about 10C for more than 3 consecutive days over the southeastern Greenland. Ice melt over this area of Greenland was detected in the brightness temperature observations.

Plain Language Summary This study highlights the role that the polar jet and associated atmospheric circulation plays in the transport of mineral dust from the Sahara desert to the Arctic across eastern side of the North Atlantic Ocean. The poleward transport of dust following this newly identified path was caused by a meandering polar jet stream that was at the origin of both dust emission (through cyclogenesis over Northwest Africa) and poleward transport of the uplifted dust toward the Arctic (through circulation related to cut-off low formation). The polar jet stream has been identified as the main driver for such events leading to the transport of large amount of dust to high-latitudes. If the polar jet is set to slow more frequently due to the changes in the Arctic climate system and to the Arctic Amplification, such events are expected to become more frequent.

1. Introduction

During the last few decades, the Arctic region has been subject to rapid changes; the Arctic climate system being more sensitive to climate change than the lower latitudes, a feature known as "Arctic amplification" (Serreze & Francis, 2006), of which the physical origin and consequences are still not completely understood. The Arctic has warmed by more than 1 °C over the last century, a rate almost twice the global average (Richter-Menge et al., 2018). At the same time, the sea ice cover has decreased rapidly, e.g., in 2007 the observed sea ice autumn minimum was 38% smaller than the climatological mean of 1979–2007 (Comiso et al., 2008) and the perennial sea ice cover lost about 50% of its extent during the 1979–2012 period (Meier et al., 2014). This trend was confirmed by Comiso et al. (2017) who used four different techniques and showed that the ice extent of the Arctic perennial ice is indeed declining at the rate of about 11% per decade. Additional changes such as retreating glaciers and the thawing of permafrost are reported (e.g. Stroeve et al., 2017). Global climate models (GCMs) have difficulty reproducing the observed Arctic warming (Shindell & Faluvegi, 2009) and the rate of observed Arctic sea ice loss (Stroeve et al., 2006). Recent studies suggest that GCM simulations of Arctic warming can be improved by better accounting for aerosols

radiative forcing (Bintanja & Krikken, 2016; Law & Stohl, 2007; Mickley et al., 2004; Quinn et al., 2008; Shindell et al., 2007).

Aerosols perturb the radiative balance of the Arctic directly by scattering, absorbing and emitting radiation, and indirectly by providing a source of cloud condensation nuclei and ice nuclei (Qian et al., 2015). Also, deposition of absorbing aerosols to the snowpack or ice reduces surface albedo and accelerates snow melt (Box et al., 2012; Kylling et al., 2018). Tedesco et al. (2014) and Dumont et al., (2014) have shown that the Greenland Ice Sheet albedo has declined substantially in recent decades due to the increase in the deposition of light-absorbing impurities, particularly dust and black carbon. Although some studies have hypothesized that dust may be darkening the ablation zone in southwest Greenland in particular, the quantification of the relative importance of black carbon, dust and other darkening agents in these regions is still to be made (Tedesco et al., 2015). Recently, Ryan et al. (2018) have demonstrated that distributed surface impurities, constituted of an admixture of dust, black carbon and pigmented algae, explain 73% of the observed spatial variability in albedo and are responsible for the Greenland dark zone itself.

Coarse size aerosol particles such as dust act like greenhouse gases by absorbing and emitting longwave (LW) radiation (Gutman & Reissell, 2011). The LW radiation plays a particularly important role in the energy balance in the Arctic because of prolonged polar nights with little or no sunlight. The aerosol effect in LW radiation in the Arctic differs from other regions because of the cold atmospheric temperatures, frequent occurrences of temperature inversion, and low water vapor amount and it is enhanced by the highly reflective snow and ice-covered surface (Gutman & Reissell, 2011). Kylling et al. (2018) quantified the instantaneous radiative forcing (IRF) of mineral dust in the Arctic for the year 2012 using dust load estimates from Groot Zwaaftink et al. (2016). They found that annual mean top of the atmosphere IRF is 0.225 W m $-$ 2, with the largest contributions from dust transported from Africa and Asia south of 60°N and that mineral dust deposited on snow accounts for nearly all of the bottom of the atmosphere IRF of 0.135 W m $-$ 2.

Overall, through direct interactions with SW and LW radiation, aerosol particles can affect the radiative balance at the top of the atmosphere, the energy balance at the surface, as well as that within the atmosphere by providing a radiative heating (or cooling) in the aerosol-laden layers (Gutman & Reissell, 2011). At the same time, aerosols indirect radiative forcing in the Arctic seems to play an important role. A recent study by Bennartz et al. (2013) has shown that low-level clouds consisting of liquid water droplets, played a key role in the historically rare period of extended Arctic sea ice melting in July 2012. Via their radiative effects, these liquid-containing clouds that occur 30 to 50% of the time across the Arctic, tend to increase near-surface temperatures and increase sea ice melting. They also demonstrated that GCMs have difficulties in simulating the Arctic surface energy budget, particularly as they tend to under-predict the occurrence fraction of optically thin liquid clouds and their radiative properties, which depend highly on aerosols concentration and properties.

In summary, through direct (including the surface albedo effect) and indirect forcing, aerosols in the Arctic can affect the main components of the atmosphere and cryosphere such as aerosol-induced changes in clouds, precipitation, sea-ice and land snow cover and hence play an important role in the Arctic climate system (Gutman & Reissell, 2011). Despite concentrated efforts to improve the quantification of the overall impact of aerosols in the Arctic (e.g., IPCC, 2007), this remains a challenging problem since it requires an adequate representation of Arctic aerosols in models, which is difficult because of their variable lifetime in the atmosphere and complex source and sink processes (e.g. IPCC, 2014).

The average lifetime in the atmosphere of aerosol particles varies from days to weeks, but they exhibit a longer lifetime in the Arctic and a marked annual cycle with maximum concentrations during the Arctic haze season, which occurs in late winter and spring (Gutman & Reissell, 2011). Aerosols transported to the Arctic can accumulate during this season because of the physical, chemical, and thermodynamic characteristics of the extremely stable Arctic lower troposphere, which tends to slow dry and wet removal processes of aerosols from the atmosphere (Gutman & Reissell, 2011). The characterization of this specific Arctic aerosol dynamic along with the evaluation of aerosol concentrations and an accurate representation of their seasonal distributions are crucial for the understanding of the aerosol impact upon the Arctic system (Hansen & Nazarenko, 2004; Quinn et al., 2008).

An important contribution to Arctic aerosol loads comes from mineral dust and it has been suggested that dust contributes to the Arctic amplification (Lambert et al., 2013, and references therein). In spring, the

observed concentrations of aerosols at Arctic surface stations reach their maximum (Breider et al., 2014; Stohl, 2006). This spring peak phenomenon extends to the entire Arctic and to all altitudes and it is commonly called "Arctic haze". Dust concentrations during Arctic haze are generally an order of magnitude higher than during summer (Quinn et al., 2007). Groot Zwaaftink et al. (2016) showed that dust loads are largest in spring when remote dust originating from Africa and Asia is efficiently transported into the Arctic, whereas the contribution of local sources is more important during fall and influences especially the surface concentrations and dust deposition.

The majority of mineral dust aerosols are thought to be transported to the Arctic from the arid and semi-arid regions located in Asia and Northern Africa (Gutman & Reissell, 2011; Groot Zwaaftink et al., 2016). The relative contribution of the Sahara and the Asian deserts (Taklamakan and Gobi) was evaluated by Breider et al. (2014) using two sensitivity simulations with dust emissions from these regions independently switched off. The results of this study showed that, on an annual basis, the Sahara is responsible for 65% of the total dust load in the Arctic and that, particularly during spring, mineral dust has a dominant Saharan source. They estimated 60% of Arctic dust in spring from the Sahara, 22% from the Taklamakan and Gobi deserts, and 18% from other deserts. Furthermore, their simulations suggest a significant role of dust in shortwave absorption both in the snowpack and in the atmosphere. They found that light absorption by Organic Carbon and dust in spring and summer contributes to 24% of the Arctic Absorbing Aerosol Optical Depth at 550 nm and dust deposition contributes to 25% of the total deposited absorption mass in spring and 10% in summer over the scale of the Arctic and for the year 2008.

Additionally, previous chemical and back-trajectory analyses point to evidence of transport of Saharan dust to the Arctic either through transport across Northern Europe or across the Atlantic Ocean around the Bermuda High (Ansmann et al., 2003; Franzén et al., 1994; Rodríguez et al., 2012; VanCuren et al., 2012). Few individual episodes of Saharan transport toward the Arctic have been documented in the last 10 years. Barkan and Alpert (2010) reported an unusual synoptic situation causing a rare event of poleward Saharan dust transportation during which the dust was observed to the northern tip of the Scandinavian Peninsula in early August 2007 in both ground based lidar and in situ measurements. Bégue et al., 2012 examined the long-range transport of Saharan dust in spring 2008 over northwestern Europe. The total dust amount emitted during this event was estimated at 185 Tg. Analysis of the removal processes over Northwestern Europe revealed that wet deposition was the main process of dust removal (73 Tg). McAuliffe and Ruth (2013), via ground based lidar measurements over Southern Ireland, documented dust transport from the Sahara in late April 2011 where a thick layer of dust extending from 0.5 to 2 km in altitude was detected by the Cork Raman Lidar.

Although Saharan dust aerosols seem to play an important role in the functioning of the Arctic system, there have been very few comprehensive studies performed to date to establish the linkages between sources, transport and spatial distributions of Saharan mineral dust in the Arctic. The magnitude of the influence in the Arctic of the Sahara - the world's most important dust source area - is still to be evaluated.

North Africa provides an estimated dust production of 50% of the global annual total (Engelstaedter et al., 2006; Laurent et al., 2008). The dust emitted by the North African sources affects many adjacent continental and ocean/sea regions. Although the majority of the dust is transported westward across the Atlantic Ocean toward the Americas (e.g. Bou Karam et al., 2008; Prospero et al., 2002), a part of the dust, mainly during spring, is transported northward into southern, central and northern Europe (Papayannis et al., 2008). Two main features influence the dust transport from North Africa to Europe; the southward trough that emanates from the Icelandic low pressure and the subtropical high over northern Africa. The strength and position of these two systems define the direction and the potential to carry dust northward which, in some cases, reaches the shores of the Baltic Sea and the Arctic (Ansmann et al., 2003; Barkan et al., 2004; Barkan & Alpert, 2010).

For Saharan dust emission, numerous atmospheric processes on synoptic, regional and local scales provide the meteorological conditions throughout the year suitable for dust mobilization over areas rich in erodible material. It is the combination of sources rich in erodible material, energetic wind systems, and a coupling to wind system that facilitate long-range transport (Barkan & Alpert, 2010). Dust storms have been documented to be associated with high near-surface winds resulting from the downward mixing of momentum from the nocturnal low-level jets (LLJs) that blow over the Sahara throughout the year (e.g. Bou Karam et al., 2017; Todd, Bou Karam, et al., 2008; Washington & Todd, 2005). Additionally, in winter, dust emission over the

Sahara has been shown to be connected with the low level dynamics associated with the penetration of an upper-level trough to low latitudes (e.g. Cavazos et al., 2009; Knippertz & Fink, 2006; Tulet et al., 2008), or to density currents caused by strong evaporational cooling along precipitating cloud-bands over the northern Sahara (Knippertz & Fink, 2006) and along the Sahara side of the Atlas Mountain chain in southern Morocco (Knippertz et al., 2007). In summertime, in addition to the LLJ related dust emissions, large outbreaks of dust over North Africa are associated with cold pools emanating from the outflow of mesoscale convective systems (MCSs) (Bou Karam et al., 2014; Sutton, 1925, 1931; Williams et al., 2009). They represent an efficient mechanism for: (i) dust mobilization by virtue of their strong near-surface winds, and (ii) dust injection to altitudes favorable for long-range transport due to the turbulent upward mixing (e.g. Bou Karam et al., 2008; Flamant et al., 2007; Marsham et al., 2013). Moreover, Bou Karam et al. (2008), Bou Karam, Flamant, Knippertz, et al., (2009), Bou Karam, Flamant, Tulet, et al., (2009) have identified another mechanism for dust emission during summer, in which highly turbulent winds at the leading edge of the monsoon nocturnal flow in the InterTropical Front (ITF) region generate dust uplifting and transport to high altitude.

Furthermore, in late winter and spring time, heavy dust storms over North Africa, have been reported to be associated with Saharan cyclones (Bou Karam et al., 2010; Schepanski et al., 2009; Westphal et al., 1985). The development of these depressions, mostly in the lee of the Atlas Mountains, is favored by the strengthening of the meridional temperature gradient over northern Africa at this time of the year (e.g. Bou Karam et al., 2010). About 25% of the total dust emissions in spring over North Africa are due to the occurrence of Saharan cyclones (e.g. Fiedler et al., 2014). The majority of these cyclones moves eastward following the coast line of the African continent. This trajectory is mainly favored by the presence of the subtropical jet at about 7 km in altitude over Africa during this period of the year (see Bou Karam et al., 2010 for more details). Flaounas et al. (2015) conducted a study over 8 years on the dust transport over the Mediterranean region. They found that Saharan cyclones are the main atmospheric systems that cause extreme dust transport events in the Mediterranean region, especially its eastern side. They showed that up to 20% of dust events, are related to Saharan cyclones and that when considering only extreme dust events, the contribution of Saharan cyclones reached 70%. More importantly, Bou Karam et al. (2010) have estimated the load of dust emitted by a single Saharan cyclone to range between 2 to 8 Tg per day.

Despite their effective role in dust emission and transport over long distance, no attention has been given to Saharan cyclones that propagate poleward. In this study, we document an extreme case of dust emission by a Saharan cyclone that occurred over Morocco on 4 April 2011 and moved poleward, transporting heavy dust plumes over the Iberian Peninsula, the northern Atlantic Ocean toward Ireland and Greenland. The purpose of this study is three-fold: (i) examine dust emission and transport toward the Arctic in connection with the Saharan cyclogenesis event of April 2011. (ii) Determine the meteorological conditions that favor a poleward propagation of the Saharan cyclone instead of the expected eastward move. (iii) Estimate dust emissions and loads associated with this event and evaluate its impact over Greenland. The paper is structured as follows: Section 2 details the datasets utilized in this study, including the numerical modeling setup. In section 3 the meteorological conditions accompanying the event are described. Section 4 details the cyclone formation and the associated dust emission. The spatio-temporal evolution of the dust storm and the estimate of dust loads emitted by the cyclone and those deposited in Arctic are provided in section 5. Section 6 provides a summary and conclusions.

2. Data Sources

2.1. Space-Borne Observations

Observations at high spatio-temporal resolution from the Spinning Enhanced Visible and Infrared Imager (SEVIRI) on board the Meteosat Second Generation (MSG-SEVIRI) geostationary satellite are used in this study in order to characterize qualitatively the dust activity over North Africa associated with the Saharan cyclone and the transport toward the Arctic. The MODIS Aqua Aerosol Product (MOD04, Levy et al., 2015) is used to acquire the daily aerosols optical depth at 1330UTC associated with the cyclone. This product accounts for the aerosol size distribution over the oceans and the aerosol type over the continents. "Fine" aerosols (anthropogenic/pollution) and "coarse" aerosols (natural particles; e.g., dust) are also included. Daily Level 2 (MOD 04) data are produced at the spatial resolution of a 10 x 10 1-km (at nadir) pixel array. The MODIS aerosol

product includes the "deep-blue" algorithm recently developed to get aerosol optical thickness over bright land areas (i.e the desert) (Hsu et al., 2013).

The horizontal distribution of dust is described using the SEVIRI images computed from a combination of three infrared channels, namely channel 10 (12 μm), channel 9 (10.8 μm) and channel 7 (8.7 μm). MSG-SEVIRI is located geostationary at 0°W over the equator and provides images of Africa on a 15-minute temporal resolution. False-color images are created using an algorithm developed by EUMETSAT which colors red the difference between the 12.0 and 10.8 μm channels, green the difference between the 10.8 and 8.7 μm channels and blue the 10.8 μm channel (e.g. Schepanski et al., 2007). On these composite images, dust appears pink or magenta and cloud appear orange or brown. Note that the dust effect on brightness temperature differences depends on its altitude (e.g. Pierangelo et al., 2004) suggesting that these composite images may favor the dust which is elevated so that its radiating temperature differs significantly from the ground. The ice melt over Greenland is inspected using the 25 km resolution AMSR-E Brightness temperature (TB) product at 36 GHz horizontal polarization for the night path (around 0100 UTC) on board the AQUA satellite. These observations have 25x25 km spatial resolution and can be downloaded from the webpage of the National Snow and Ice Data Center (Brodzik et al., 2016).

2.2. The ECMWF ReAnalysis ERA5 and Meso-NH Regional Simulation

Synoptic-scale meteorological conditions during the event under scrutiny as well as the characteristics of the cyclone were studied using 6-hourly European Centre for Medium-range Weather Forecasts (ECMWF) ReAnalyses ERA5, having a spatial resolution of 31 km globally and 137 levels to 0.01 hPa on the vertical.

The simulation was performed using the Meso-NH (version 5–3-0) atmospheric model (Lac et al., 2018; Lafore et al., 1998), a non-hydrostatic mesoscale atmospheric model with an on-line dust emission and transport module (Grini et al., 2006). The performances of Meso-NH (especially in terms of dynamics, the main factors that drives dust mobilization) are well established, and its ability to simulate dust emission and transport over North and West Africa has been highlighted in several recent studies (e.g. Bou Karam, Flamant, Knippertz, et al., 2009; Bou Karam, Flamant, Tulet, et al., 2009; Todd, Washington, et al., 2008; Tulet et al., 2008). Furthermore, the Meso-NH model has been extensively validated over north and West Africa where dust uplift associated with LLJ dynamics are observed on a regular basis all year round. It has been validated using many "aerosol related" datasets acquired from ground-based platforms (Mallet et al., 2009; Todd, Bou Karam, et al., 2008; Tulet et al., 2008), airborne platforms (Bou Karam et al. 2008; Bou Karam, Flamant, Tulet, et al., 2009; Crumeyrolle et al., 2011; Schepanski et al., 2012) and spaceborne platforms (Bou Karam, Flamant, Knippertz, et al., 2009, Bou Karam et al., 2010, 2014; Chaboureau et al., 2011)).

The model was run during 6 days from 3 April 2011 at 00 UTC to 10 April 2011 at 00 UTC over a domain of 4608 × 7680 km2 using a 24 km horizontal grid spacing covering North Africa, Western Europe and the Northern Atlantic Ocean. In the vertical, 72 levels were used with 35 of them within the planetary boundary layer (i.e. below 2 km). The lowermost level is at 10 m above the ground, while the highest level is at 28 km above the ground. The initial and boundary conditions are provided by the analysis from the European Center for Medium-Range Weather Forecasts (ECMWF).

In order to take into account both the dust and the formation of clouds associated with the cyclone, the run used a convective mass-flux scheme (Bechtold et al., 2001), a mixed-phase bulk microphysical scheme (Pinty & Jabouille, 1998), a subgrid cloud cover and condensate content scheme (Chaboureau & Bechtold, 2002, 2005), a turbulence parameterization (Cuxart et al., 2000), the Rapid Radiative Transfer Model parameterization (Mlawer et al., 1997) that takes into account the radiative effect of dust and a dust scheme (Grini et al., 2006). The later included the Dust Entrainment and Deposition (DEAD) scheme (Zender et al., 2003) that calculates dust fluxes from wind friction speeds and the ORganic and Inorganic Log-normal Aerosols Model (ORILAM: Tulet et al., 2005) in which transport, dry and wet deposition, and radiative properties of the distribution of three dust particle size are parameterized. The dust scheme has been successfully employed by Tulet et al. (2008), Bou Karam, Flamant, Knippertz, et al., (2009), Bou Karam, Flamant, Tulet, et al., (2009), Bou Karam et al., (2010, 2014), Chaboureau et al. (2011, 2016) among others.

3. The Meteorological Conditions at Synoptic Scale Leading to Cyclogenesis

As demonstrated in previous studies, North African cyclogenesis results from the combination of at least three factors. In addition to the orographic forcing that affects the nature of the cyclogenesis (e.g., Egger et al., 1995; Hare, 1943; Horvath et al., 2006), interactions between the upper-level troposphere structure and the low-level baroclinity offer the optimal conditions to trigger the growth of the Saharan lows (e.g., Thorncroft & Flocas, 1997; Trigo et al., 2002).

3.1. Upper-Level Jets

The situation at the upper levels of the troposphere (i.e. 250 hPa) before the initiation of the cyclogenesis (i.e. before April 03 at 0018 UTC) is described using the ECMWF analyses for wind speed and direction as well as temperature and potential vorticity (Figure 1). In the wind field at 250 hPa, the polar jet stream (PJS) stands out clearly between 30 and 40 N with strong southwesterly winds exceeding 60 m s-1 and a meandering shape (Figure 1a) associated with the intrusion of an upper level trough near 12 W from high latitudes. The upper-level front was associated with high values of potential vorticity exceeding 5 PVU over 100 km in width (Figure 1b). Twelve hours later, the high-latitude-upper-level trough became narrower, moved eastward and penetrated as south as 27 N at 10 W reaching the western flank of the Anti-Atlas Mountains in Morocco (Figure 1c and d).

3.2. Low-Level Temperature Gradient

Figures 1e and f show the temperature and streamlines at 925 hPa on April 3 at 06 and 18 UTC respectively. A broad baroclinic zone characterized by a strong temperature gradient of about 10 K over 1 degree in longitude is present along the Atlantic coastline in Morocco. The well-marked southwest-northeast oriented temperature gradient seen in the low levels of the atmosphere (i.e. 950 hPa, Figure 1e and f) satisfies the necessary conditions for baroclinic instability (e.g. Thorncroft & Flocas, 1997); an important precursor for Saharan cyclogenesis (e.g. Alpert & Ziv, 1989). The gradient in surface temperature was characterized by a maximum of temperature (305 K) located over the continent associated with daytime surface heating and a minimum of temperature (285 K) located over the eastern Atlantic (Figure 1e and f).

These three conditions (i.e. the upper level trough, orography and temperature gradient), qualified as optimal for Saharan cyclogenesis (e.g. Trigo et al., 2002), triggered a Saharan low on April 4, 2011 at 0000UTC in the lee of the Anti-Atlas Mountains close to 27°N/9°W (Figure 1f). The cyclone developed at low levels within the region of strong baroclinity (Figure 1e) and in the presence of the upper level trough (Figure 1 b and d) perturbed by the orography.

4. Cyclone Formation and Dust Storm

4.1. Cyclone Characteristics

The Saharan depression formed over southern Morocco in the lee of the Anti-Atlas Mountains on the midnight of 4 April in response to high-latitude-upper-level trough intrusion as discussed in the previous section. It was centered at 9 W and 27 N (Figure 1f) then it migrated westward and northward (Figure 2a and b) and dissipated over the eastern Atlantic off the Iberian coast on 6 April. The cyclone lifetime was about 3 days. It formed on 4 April at 0000 UTC and by 7 April at 0000 UTC no signature in the MSLP field of the cyclone can be seen (not shown); by this time the cyclone has merged with the main stream over the Atlantic Ocean as will be discussed in section 5.

The cyclone was characterized by a surface pressure anomaly of about 9 hPa at its center with respect to the environment (not shown). The center of low pressure associated with the cyclone deepened with time and on the evening of 4 April the surface pressure anomaly at its center reached 12 hPa (Figure 2a), and the potential vorticity exceeded 6 PVU on 5 April at 1200UTC (Figure 2b).

The cyclone was characterized by a warm front east of the low typified at the surface by temperatures higher than 300 K, and a sharp cold front characterized by surface temperatures less than 290 K (Figure 2d). The strongest winds are located in the regions of strong temperature gradient (Figure 2c) and they exceeded 20 $m.s^{-1}$.

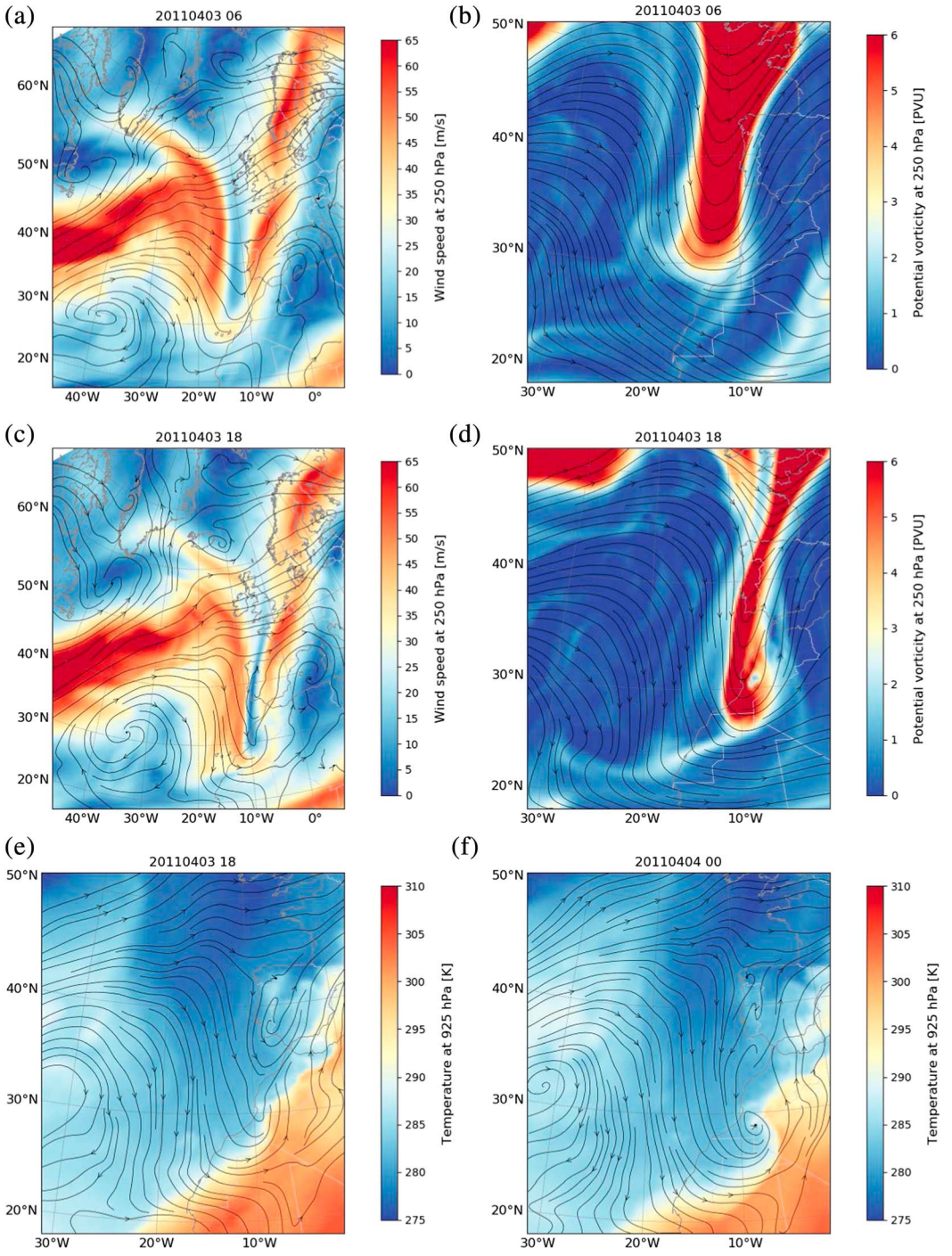

Figure 1. ECMWF ERA5 reanalyses at 250 hPa on 03 April at 0600UTC of wind speed a and potential vorticity b. c same as a and (d) same as (b) but for 1800UTC. E and f are ERA5 reanalyses for temperature at 925 hPa for 03 April 2011 at 1800UTC and 04 April 2011 at 0000UTC respectively. Wind direction at 700 hPa is superimposed on all the figures by the black streamlines.

4.2. Dust Emission and Transport

The cyclone provided a dynamical forcing that led to strong near-surface winds exceeding 20 $m.s^{-1}$ and produced a major dust storm over North Africa as recorded by SEVIRI satellite shown in Figure 3. The dust was transported all around the cyclone (pink colors, Figure 3a and 3b) leaving a clear eye at its center and was

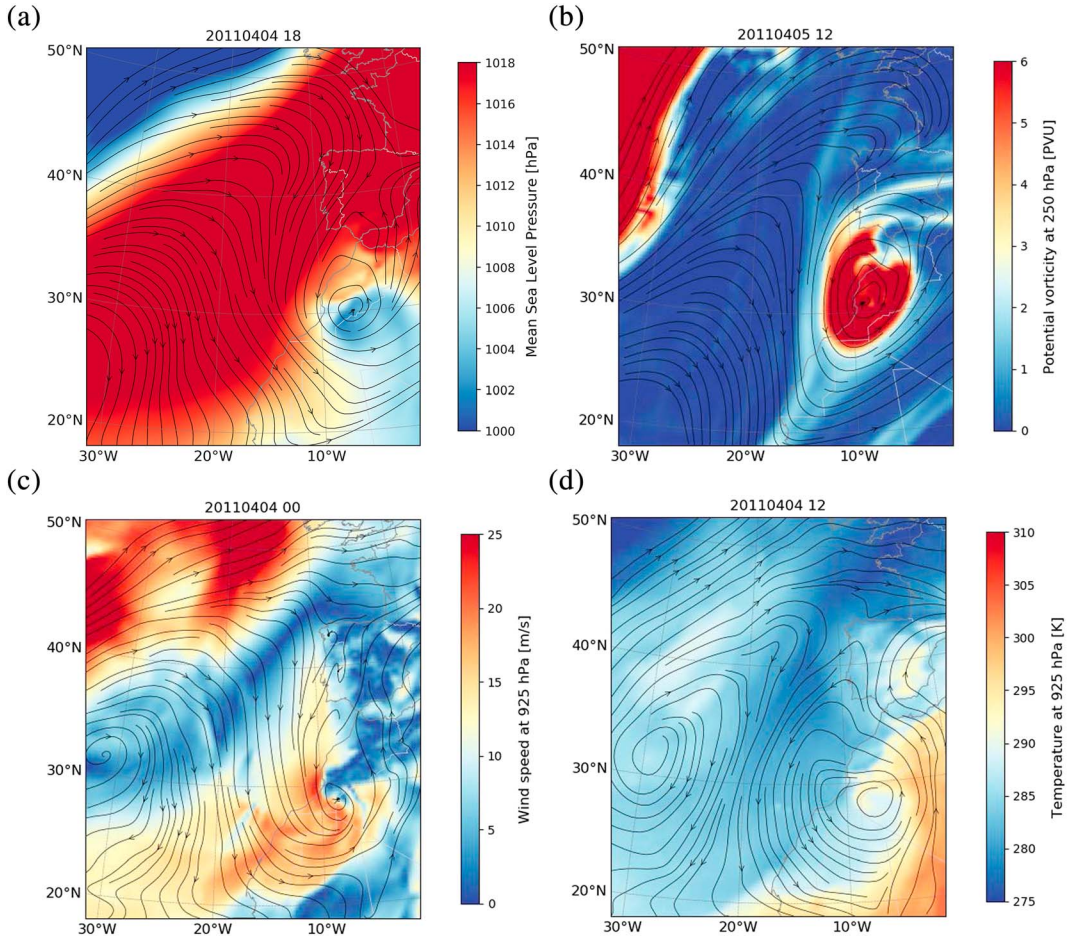

Figure 2. ECMWF ERA5 reanalyses of mean sea level pressure (colors) and wind direction at 700 hPa (streamlines) on 04 April 2011 a at 1800UTC. Potential vorticity at 250 hPa (colors) and wind direction at 700 hPa (streamlines) on 05 April 2011 at 1200 UTC b. wind speed at 925 hPa (colors) and wind direction at 700 hPa (streamlines) on 04 April 2011 at 0000 UTC c. temperature at 925 hPa (colors) and wind direction at 700 hPa (streamlines) on 04 April 2011 at 1200 UTC d.

accompanied by a thick high-level cloud band along the northern edge of the cyclone (dark red colors, Figure 3a and 3b). On the vertical, slanted dust layers reaching 6 km in altitude were observed in the CALIPSO satellite observations during this event (not shown). The cyclone provided the necessary dynamical lofting of the dust to high altitudes making it subject to long range transport.

The dust from the Saharan cyclone expanded several thousand kilometers over the east side of the North Atlantic and southwestern Europe in April 2011 (Figure 3c, 3d). The low-pressure system intensified with time and channeled the dust west and then north, resulting in a thick circular dust cloud stretching more than 15 degrees in latitude and in longitude (Figure 3c and 3d).

The dust cloud continued to spread both northward and westward. It was seen to cover most of Western Europe and eastern North Atlantic on 7 and 8 April 2011 (Figure 3e and 3f). The part of the dust cloud located over the ocean was also pushed northward. It passed over Ireland on 8 April at 2100UTC, where a layer of dust located between 2 and 3 km was detected in the lidar measurements at the Cork Raman Lidar station in southern Ireland (51.8933 N, −8.4942 E, 75 m, not shown), and it reached Greenland the day after as inferred by the model simulation (since Greenland is outside the coverage area of SEVIRI) which will be discussed in section 5.

(brown/red) and differences in surface emissivity retrieved in absence of dust or clouds (light blue/blue) on: (a) 05 April 2011 at 0600 UTC, (b) 05 April 2011 at 1800 UTC, (c) 06 April 2011 at 0300 UTC, (d) 06 April 2011 at 0600 UTC, (e) 07 April 2011 at 0600 UTC and (f) 08 April 2011 at 0000 UTC.

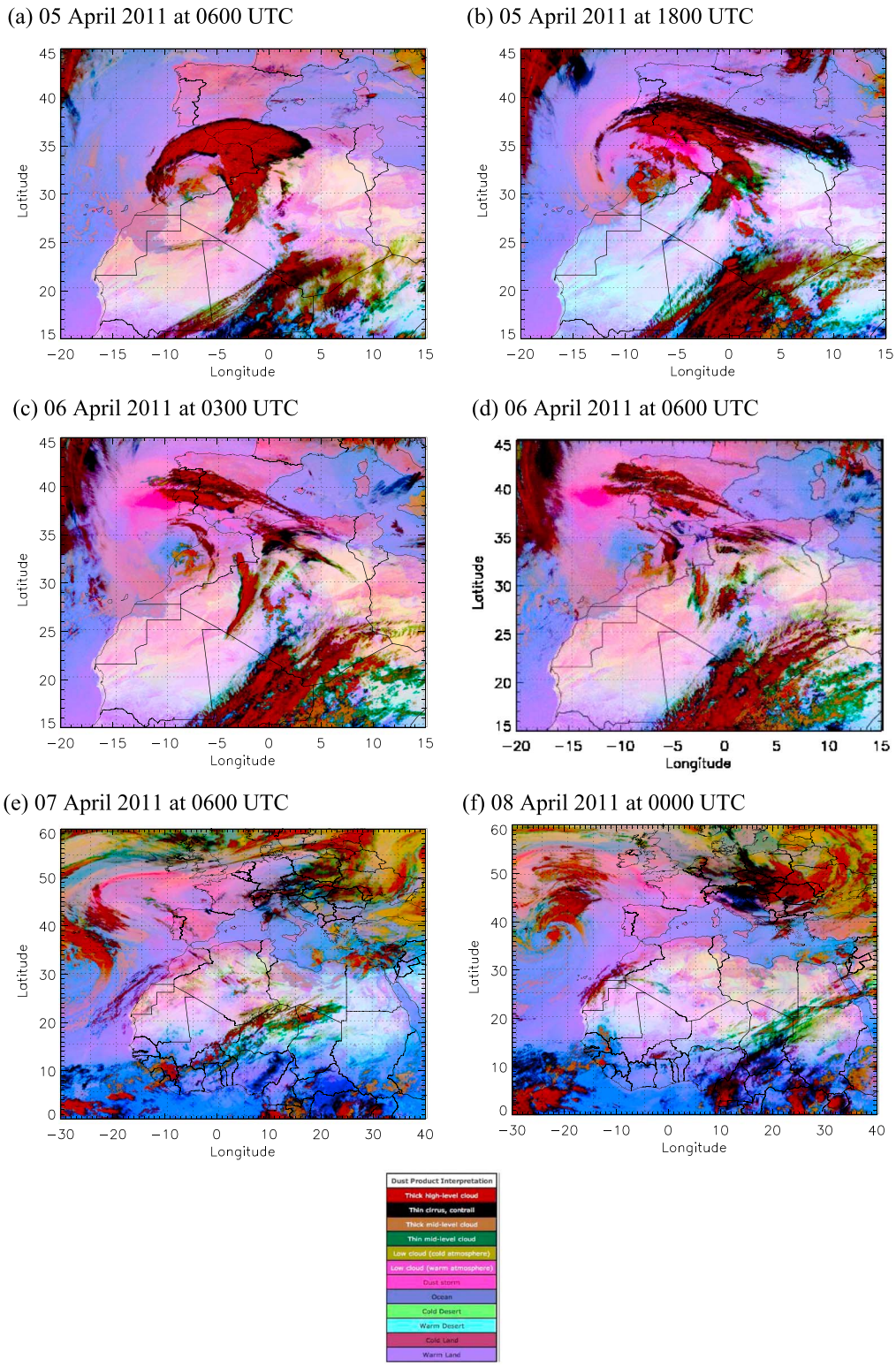

Figure 3. SEVIRI-derived false color images over North Africa, showing dust (pink), clouds.

4.3. Mechanism by which the Dust Was Transported Poleward

We discussed in the previous section how a first meander of the polar jet stream led to the intrusion of an upper level trough which, associated with orographic blocking, caused the cyclogenesis and dust storm to

occur over northwest Africa. In this section, we will show how a second shortwave trough of the still meandering polar jet stream is driving the poleward transport of dust.

It is known that when the polar jet stream slows it meanders in a waveform pattern that allows the extension of low pressure lobes and cold fronts much further to the south. The intrusion of low pressure lobes to mid-latitudes can develop and finally detach from the polar jet in a 'drop' of cold air via a process called cut-off. These low pressure lobes can become stationary for few days and block the normal circulation of the atmosphere before merging again with the main jet stream.

Figure 4 shows respectively a shortwave trough of the polar jet stream developing on 6 April 2011 (a) then finally detaching a cut-off low on 7 April 2011 (b). When the cut-off occurred on 7 April, the dust cyclone created 2 days earlier by the first polar jet's meander, had reached the coast of France and was blocked in this location by the downstream ridge (Figure 4c and 4d). The two features are seen as a high and a low side by side in the geopotential height field at 500 hPa (Figure 4d) as well as in the streamlines field at 700 hPa (Figure 4c). The following day the dust cyclone and the lobe of low pressure merged together (Figure 4e and Figure 4f) and then merged with the main jet stream. The polar jet stream is now carrying the dust northward during the following few days (i.e. Figure 3f). The consecutive shortwave troughs of the polar jet stream, not only generated the dust storm over Africa but also favored its transport far north.

5. The Impacts of this Event

5.1. Estimation of the Dust Load and Deposition

In order to estimate the dust load and deposition, we make use in this section of the outputs of the MesoNH model simulation. A first step consists of validating the model results in terms of aerosol optical depth (AOD) against observations in order to discuss later with confidence the other parameters. A comparison of AODs derived from MODIS deep blue satellite observations and simulated by the model shows good agreement (Figure 5a). The model was able to reproduce the structure, the lifetime, and the trajectory of the cyclone and the associated dust. This agreement between model and observations suggests that the model can be used reliably to quantify the dust emissions and deposition associated with this event. AOD values as large as 2 were associated with the dust around the cyclone. Both the observed and simulated AODs decreased with time and with latitude due to dust deposition during the transport. The dust cloud that reached Greenland was associated with an AOD of about 0.5 (Figure 5a). By the end of the episode, a total dust load of 38.35 Tg was carried to areas located north of 40 N, and dust deposition was estimated at 1.3 $x10^{-3}$ Tg to the north of 40 N (Figure 5b and 5c). For the Arctic region i.e. areas to the north of 60 N, the dust load was 16.54 Tg and the deposition was 0.11 x10–3 Tg (Figure 5b and 5c). These results suggest that dust emissions linked to Saharan cyclones and dust import associated with the polar jet may contribute significantly to the total dust loads in the Arctic observed annually. However, a longer simulation for at least one year and over a bigger domain covering the whole arctic is needed to be able to estimate the percentage to which such an event contributes to the annual dust load in the Arctic found in the literature (e.g. Breider et al., 2014).

5.2. Characteristics of Air Masses Over Greenland and Ice Melt

The air masses over Greenland associated with this event had three main characteristics; they were loaded with dust, warm, and humid. Figure 6 shows Hovmöller plots of the simulated dust load and the ERA5 reanalysis of 2 m air temperature and total column water vapor average over longitudes 30 to 50 W. A narrow dust plume carrying dust load of about 0.6 Tg is seen to advance northward starting on 7 April 2011 at 55 N and reaching 80 N by 9 April 2011 (Figure 6a). The Hovmöller of 2 m air temperature shows a band of 10C warm air masses between 55 N and 62 N during the event (6 to 9 April). Further north, intrusion of warm air beyond 67 N is seen to happen between 8 and 11 April. Air masses warmer by 10C than the previous and following days can be seen to reach these latitudes during 8–11 April (Figure 6b). In the total water vapor column Hovmöller plot, a similar pattern to the dust load plot can be seen, characterized by a narrow area of moist air stretching northward during 7–9 April (Figure 6c).

The increase by 10C in surface air temperature over 3 days associated with the arrival of the dusty-warm-moist air masses from mid-latitudes to the southeastern parts of Greenland is also seen in the ERA5 fields of 2 m air temperature for the 9–11 period (Figure 7a, 7c, and 7e).

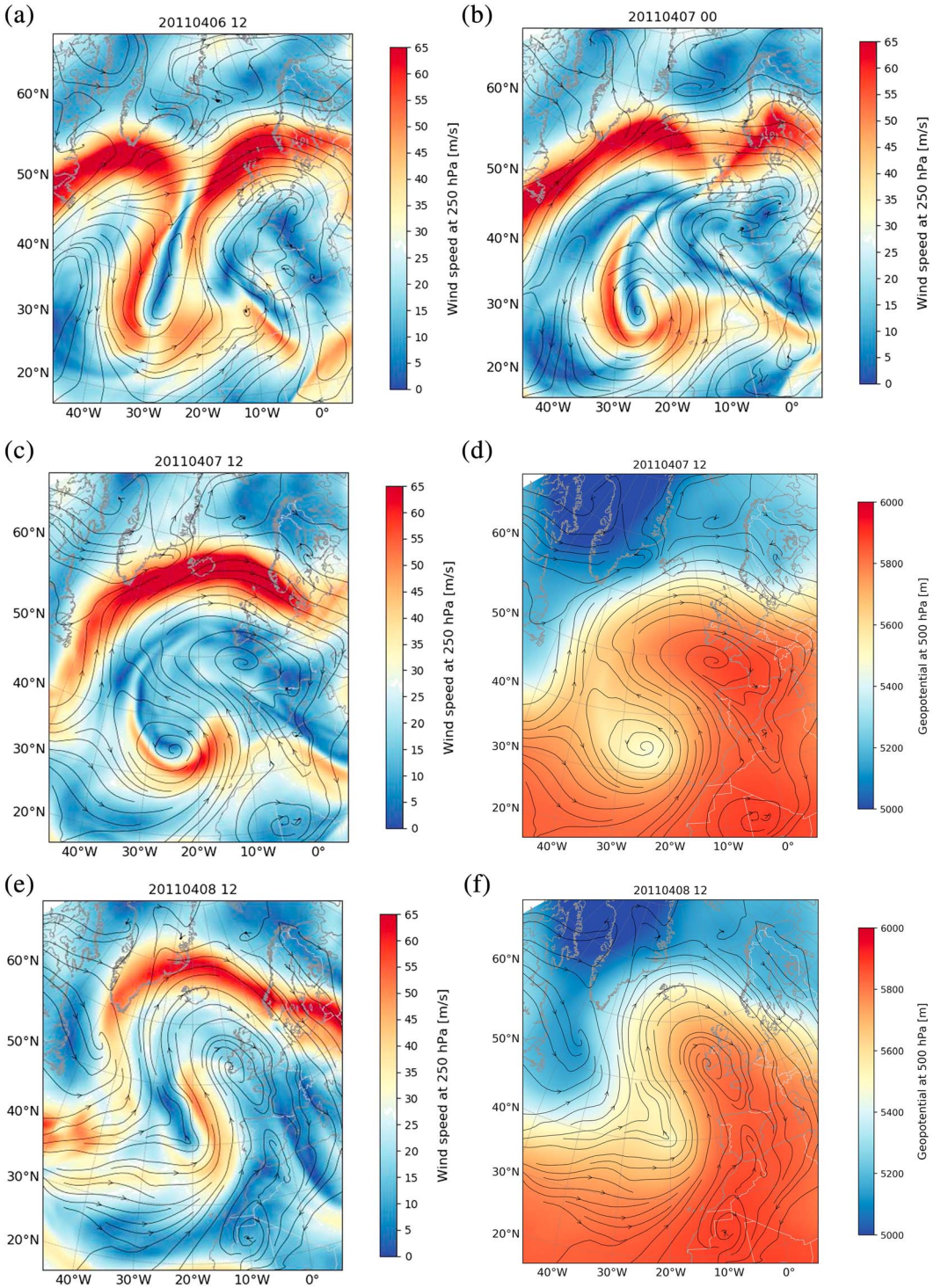

Figure 4. ECMWF ERA5 reanalyses of wind speed at 250 hPa (colors) and wind direction at 700 hPa (streamlines) on a 06 April 2011 at 1200 UTC, b 07 April 2011 at 0000 UTC, c 07 April 2011 at 1200 UTC and e 08 April 2011 at 1200 UTC. ECMWF ERA5 reanalyses of geopotential height at 500 hPa (colors) and wind direction at 700 hPa (streamlines) on (d) 07 April 2011 at 1200 UTC and and f 08 April 2011 at 1200 UTC.

Ice melt during the same period was detected over southeast Greenland from both ground based and satellite measurements of brightness temperature (TB). By checking the recorded TB values at the MIT PROMICE station in east Greenland (65.692 N 37.83 W near Tasiilaq, i.e. yellow circle in Figure 7) ice melt was seen to

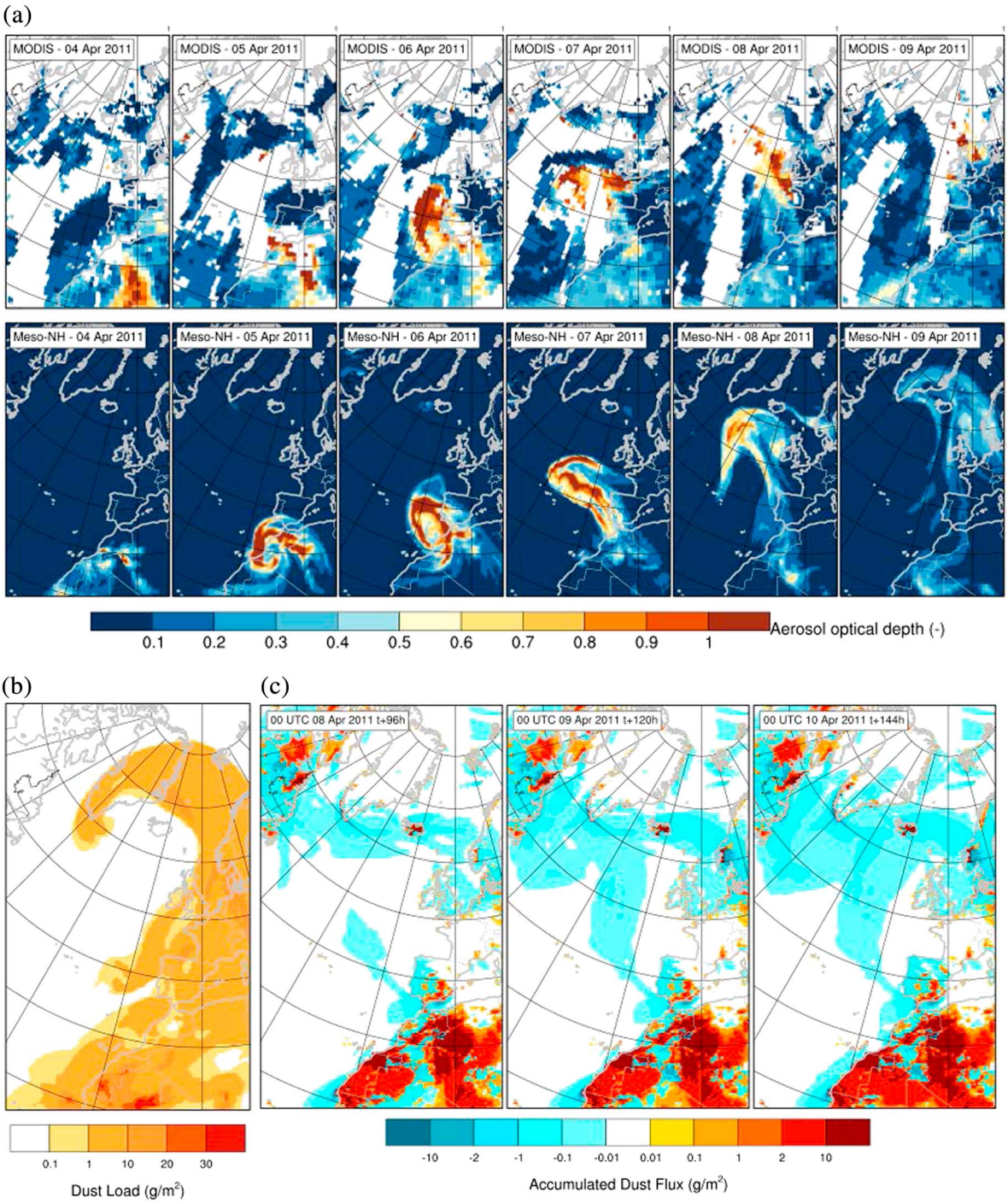

Figure 5. A daily AOD derived from MODIS AQUA observations at 1330UTC at the equator (top) and daily simulated AODs by MesoNH at 12UTC (bottom). The white areas in MODIS observations indicate areas where no data were available. B the spatial distribution of dust load on 10 April 2011 0000UTC accumulated over the whole period of simulation. C accumulated dust deposition on the 8th, the 9th and the 10th. The latest represents the accumulation over the whole period of the simulation (3–10 April 2011). Negative values in dust fluxes represent dust deposition.

occur on April 10, 2011 when the 36HGz TB reached 242.7 K, which exceeded the melt threshold around this location equal to 239.6 K (e.g., Mote, 2007; Mote & Anderson, 1995).

Satellite observations of brightness temperature over Greenland acquired from the AMSR-E satellite for the period 9–11 April 2011 (Figure 7b, 7d and 7f) indicated that the TB of the ice cover over southeast

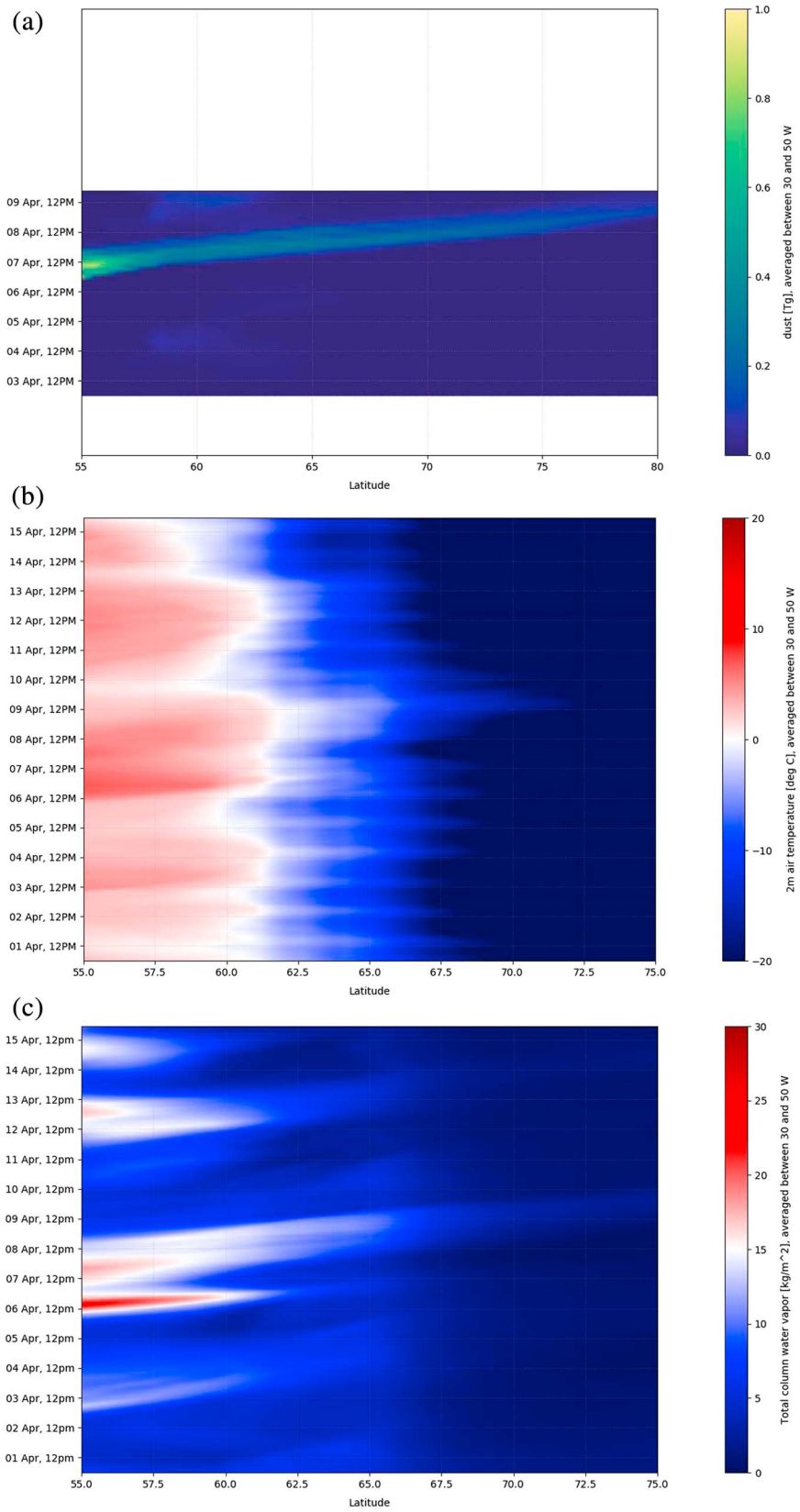

Figure 6. A Hovmöller plot of simulated dust load averaged over longitudes 30 to 50 W during the period of the simulation 3–10 April 2011. Hovmöller plot of 2 m air temperature b and total column water vapor c derived from ERA5 averaged over longitudes 30 to 50 W during 1 to 15 April 2011.

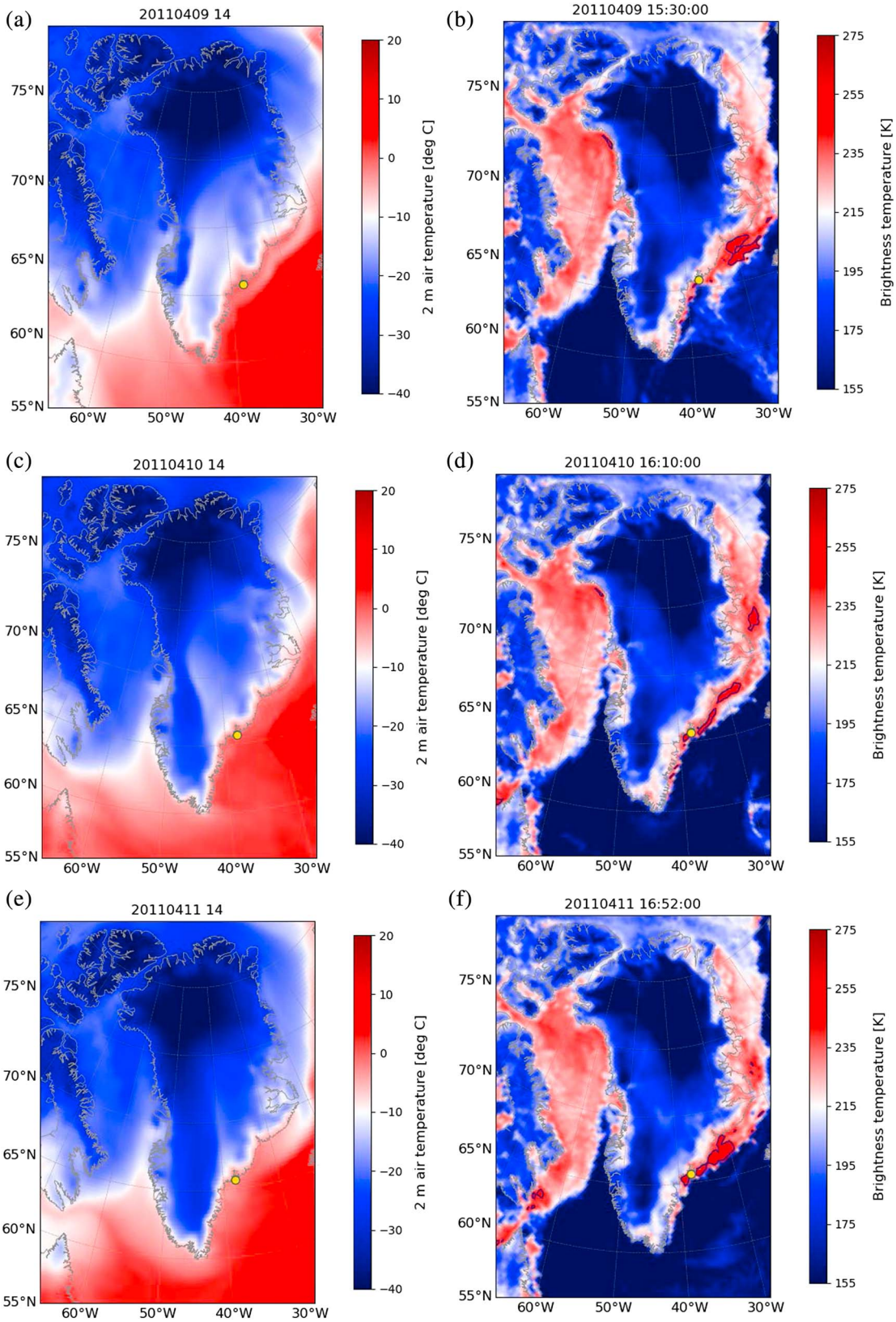

Figure 7. 2 m air temperature from ERA5 reanalysis on 9 (a), 10 (c) and 11 (e) April 2011 at 1400UTC and AMSR-E brightness temperature at 36GHz horizontal polarization for the night path (around 0100 UTC) on 9 (b), 10 (d) and 11 (f) April 2011. The yellow circle represents the position of the MIT PROMICE station and the black countour represents the threshold of 248 K set for ice melt detection in the AMSR-E data over Greenland.

Greenland increased by more than 20 K on the days of 9 and 10 April coinciding with the arrival of the warm air masses from mid-latitudes loaded with dust (i.e. Figures 3 and 5). The TB data at 36 GHz horizontal polarization for the night path (around 0100 UTC) of AMSR-E shows values between 235 and 257 K over the coastal areas during the period of interest i.e. 9 to 11 April 2011. The TB values exceeded 248 K which is the threshold corresponding to the presence of melted ice in the 36 H GHz TB AMSR-E data over Greenland (e.g. Apgar et al., 2007). This threshold is presented by the black contour in Figure 7.

Such short episodes of increase in temperature in spring (e.g., Mattingly et al., 2018) are associated punctual ice melt and could set favorable preconditions for an early ice melt onset in the Arctic where the onset of ice melt has been occurring earlier in the year over the last few decades (e.g. Stroeve et al., 2006). However, it is difficult to distinguish between the increase in temperature due to the dust radiative impact and the one due to warm air coming from mid-latitudes. For that, one should run simulation with and without dust and compare the increase of surface temperature in both simulation. This exercise is beyond the scope of this study.

6. Summary and Conclusions

This study represents an illustration of the interactions and feedbacks between high, mid-latitudes and subtropics under a particular situation linked to a meandering polar jet stream.

The shortwave troughs associated with the meandering polar jet was at the origin of both dust emission (through cyclogenesis over Northwest Africa) and poleward transport of the uplifted dust toward the Arctic (through circulation related to cut-off low formation). The dust emission was associated with an intense Saharan cyclone that formed over Northwest Africa in early April 2011. The formation of the Saharan cyclone was caused by the intrusion into subtropics of a high-latitude-upper-level trough, linked to the meandering polar jet, which initiated cyclogenesis over Northwest Africa after orographic blocking by the Anti-Atlas Mountains in Morocco. The still meandering polar jet led, two days later, to the formation of a cut-off low further south with which the Saharan dust-cyclone has merged and moved northward with the main stream of the polar jet.

Satellite observations at high spatial–temporal resolution were used to characterize qualitatively (using MSG-SEVIRI) and quantitatively (using MODIS) the dust activity over North Africa associated with the Saharan cyclone as well as the transport of dust toward the Arctic. The dust blew out from the Sahara desert in Northwest Africa on 4 April 2011, picked up by the strong winds associated with the Saharan cyclone. The tell-tale circular cloud pattern of the low-pressure system was visible in SEVIRI image during the cyclone formation and intensification. SEVIRI identified the Saharan dust off the coast of west Europe during 6–8 April 2011, as it was moving poleward.

Besides the observations, a simulation at high resolution was performed using the prognostic dust-permitting model MesoNH. The total dust load carried during this event to areas located north of 40 N was estimated by the model to be 38 Tg and dust deposition was estimated to be 1.3 Tg. This event is unusual given its scale and the amount of dust transported northward. A climatological study to quantify the frequency of such events is to be envisaged in the future. More importantly, it is crucial to represent such events in global climate models designed to estimate the role of dust in the Arctic climate system and to project future climate change of the northern pole.

Furthermore, the Saharan dust reaching Greenland was accompanied by warm and moist air masses that caused a rise in surface temperature of about 10C for more than 3 consecutive days over the southeastern Greenland. Ice melt over this area of Greenland was detected in the brightness temperature fields from both ground based and satellite observations. However, the radiative forcing of airborne dust and the changes in ice albedo due to dust deposition on ice during such an event still need to be evaluated in future studies in order to estimate the total impact of Saharan dust on Arctic ice both through melting and albedo changes. It has been long recognized that deposition of light absorbing aerosols such as dust onto snow- and ice-covered surfaces can result in a reduction of the surface SW albedo. The efficacy of the albedo effect, measured as the effectivity in increasing the surface air temperature per unit of forcing, is twice as large as that of CO2 forcing, and it may be even more effective in melting snow and ice.

In this study, we identify a new mechanism by which the dust travels over long distances across the eastern side of the North Atlantic Ocean toward the Arctic. This path is to be added to the two known paths

mentioned in previous studies i.e. through transport across Northern Europe and across the Atlantic Ocean around the Bermuda High (e.g. Rodríguez et al., 2012; VanCuren et al., 2012). Moreover, this path may be the most effective one in terms of dust load import into the Arctic given the fact that it is the shortest and most direct path. This configuration allows large amount of the uplifted dust in source area, to reach the Arctic before deposition. The poleward transport of dust following this path was caused by a meandering polar jet stream, which led to cut-off low further south with which the Saharan cyclone has merged and moved northward following the main stream of the polar jet. The polar jet stream has been identified as the main driver for such events. If the polar jet is set to slow more frequently due to the changes in the Arctic climate system, such events are expected to become more frequent. The link of Saharan dust transport to the Arctic heat dome and ice melt events need also to be investigated.

Francis and Vavrus (2012) explained how the Arctic Amplification under projected climate change can result in a slowed meandering jet stream with more cut-off and warm ridges. In this study, we demonstrated that such atmospheric circulation constitutes a favorable set for the transport of dust, warm and moist air masses from subtropics and mid-latitudes to the Arctic where approximately half of the warming is being attributed to increased moisture and heat fluxes transported to the region (McGuire et al., 2006).

In addition to their direct impact on the changes in surface temperature and on the albedo, dust aerosols have an important role in controlling the Arctic climate through altering large-scale transport of heat and moisture to the Arctic from mid-latitudes and this by modifying the global or Northern Hemisphere forcings outside the Arctic region (e.g. Shindell et al., 2007). The contribution of this aerosol-involved teleconnection to the regional changes occurring in the Arctic region remains unknown.

Acknowledgments
The European Centre for Medium-Range Weather Forecasts (ECMWF) is acknowledged for making the meteorological analyses available from their data server. The ERA5 reanalyses used in this study are available here: https://www.ecmwf.int/en/forecasts/datasets/archive-datasets/reanalysis-datasets/era5. The SEVIRI data are available on EUMETSAT data center: https://www.eumetsat.int/website/home/Data/DataDelivery/OnlineDataAccess/index.html. Karen Acheson from the Physics Department and Environmental Research Institute at the University College Cork is acknowledge for the given inputs on the lidar observations at Cork. The authors wish to thank Cyrille Flamant and Juan Cuesta for valuable discussions. This research was carried out on the High Performance Computing (HPC) resources at New York University Abu Dhabi and supported by the NYU Abu Dhabi Research Institute (G1204) in the UAE.

References

Alpert, P., & Ziv, B. (1989). The Sharav cyclone - observations and some theoretical considerations. *Journal of Geophysical Research*, *94*(D15), 18,495–18,514. https://doi.org/10.1029/JD094iD15p18495

Ansmann, A., Bösenberg, J., Chaikovsky, A., Comerón, A., Eckhardt, S., Eixmann, R., et al. (2003). Long-range transport of Saharan dust to northern Europe: The 11–16 October 2001 outbreak observed with EARLINET. *Journal of Geophysical Research*, *108*(D24), 4783. https://doi.org/10.1029/2003JD003757

Apgar, D. J., Ramage, J. M., McKenney, R. A., & Maltais, P. (2007). AMSR-E algorithm for snowmelt onset detection in sub-arctic heterogeneous terrain. *Hydrological Processes*, *21*, 1587–1596. https://doi.org/10.1002/hyp.6721

Barkan, J., & Alpert, P. (2010). Synoptic analysis of a rare event of Saharan dust reaching the Arctic region. *Weather*, *65*(8), 208–211. https://doi.org/10.1002/wea.503

Barkan, J., Kutiel, H., Alpert, P., & Kishcha, P. (2004). Synoptics of dust intrusion days from the African continent into the Atlantic Ocean. *Journal of Geophysical Research*, *109*, D08201. https://doi.org/10.1029/2003JD004416

Bechtold, P., Bazile, E., Guichard, F., Mascart, P., & Richard, E. (2001). A mass flux convection scheme for regional and global models. *Quarterly Journal of the Royal Meteorological Society*, *127*(573), 869–886. https://doi.org/10.1002/qj.49712757309

Bégue, N., Tulet, P., Chaboureau, J.-P., Roberts, G., & Gomes, L. (2012). Long-range transport of Saharan dust over northwestern Europe during EUCAARI 2008 campaign: Evolution of dust optical properties by scavenging. *Journal of Geophysical Research*, *117*, D17201. https://doi.org/10.1029/2012JD017611

Bennartz, R., Shupe, M. D., Turner, D. D., Walden, V. P., Steffen, K., Cox, C. J., et al. (2013). July 2012 Greenland melt extent enhanced by low-level liquid clouds. *Nature*, *496*(7443), 83–86. https://doi.org/10.1038/nature12002

Bintanja, R., & Krikken, F. (2016). Magnitude and pattern of Arctic warming governed by the seasonality of radiative forcing. *Nature Scientific Reports*, *6*(1). https://doi.org/10.1038/srep38287

Bou Karam, D., Flamant, C., Cuesta, J., Pelon, J., & Williams, E. (2010). Dust emission and transport associated with a Saharan depression: The February 2007 case. *Journal of Geophysical Research*, *115*, D00H27. https://doi.org/10.1029/2009JD012390

Bou Karam, D., Flamant, C., Knippertz, P., Reitebuch, O., Pelon, J., Chong, M., et al. (2008). Dust emissions over the Sahel associated with the west African monsoon inter-tropical discontinuity region: A representative case study. *Quarterly Journal of the Royal Meteorological Society*, *134*, 621–634.

Bou Karam, D., Flamant, C., Knippertz, P., Reitebuch, O., Pelon, J., Chong, M., et al. (2009). Dry cyclogenesis and dust mobilization in the inter tropical discontinuity of the west African monsoon: A case study. *Journal of Geophysical Research*, *114*, D05115. https://doi.org/10.1029/2008JD010952

Bou Karam, D., Williams, E., Janiga, M., Flamant, C., McGraw-Herdeg, M., Cuesta, J., et al. (2014). Synoptic scale dust emissions over the Sahara desert initiated by a moist convective cold pool in early august 2006. *Quarterly Journal of the Royal Meteorological Society*, *140*(685), 2591–2607. https://doi.org/10.1002/qj.2326

Bou Karam, D. B., Flamant, C., Tulet, P., Chaboureau, J.-P., Dabas, A., & Todd, M. C. (2009). Estimate of Sahelian dust emissions in the inter-tropical discontinuity region of the west African monsoon. *Journal of Geophysical Research*, *114*, D13106. https://doi.org/10.1029/2008JD011444

Bou Karam, F. D., Flamant, C., Chaboureau, J.-P., Banks, J., Cuesta, J., Brindley, H., et al. (2017). Dust emission and transport over Iraq associated with the summer Shamal winds. *Aeolian Research*, *24*, 15–31. https://doi.org/10.1016/j.aeolia.2016.11.001

Box, J. E., Fettweis, X., Stroeve, J. C., Tedesco, M., Hall, D. K., & Steffen, K. (2012). Greenland ice sheet albedo feedback: Thermodynamics and atmospheric drivers. *The Cryosphere*, *6*(4), 821–839. https://doi.org/10.5194/tc-6-821-2012

Breider, T. J., Mickley, L. J., Jacob, D. J., Wang, Q., Fisher, J. A., Chang, R. Y.-W., et al. (2014). Annual distributions and sources of Arctic aerosol components, aerosol optical depth, and aerosol absorption. *Journal of Geophysical Research: Atmospheres*, *119*, 4107–4124. https://doi.org/10.1002/2013JD020996

Brodzik, M. J., Long, D. G., Hardman, M. A., Paget, A., and Armstrong, R. (2016). MEaSUREs Calibrated Enhanced-Resolution Passive Microwave Daily EASE-Grid 2.0 Brightness Temperature ESDR, Version 1. [AMSRE]. Boulder, Colorado USA. NASA National Snow and Ice Data Center Distributed Active Archive Center. https://doi.org/10.5067/MEASURES/CRYOSPHERE/NSIDC-0630.001

Cavazos, C., Todd, M. C., & Schepanski, K. (2009). Numerical model simulation of the Saharan dust event of 6–11 march 2006 using the regional climate model version 3 (RegCM3). *Journal of Geophysical Research*, *114*, D12109. https://doi.org/10.1029/2008JD011078

Chaboureau, J.-P., & Bechtold, P. (2002). A simple cloud parameterization derived from cloud resolving model data: Diagnostic and prognostic applications. *Journal of the Atmospheric Sciences*, *59*(15), 2362–2372. https://doi.org/10.1175/1520-0469(2002)059<2362:ASCPDF>2.0.CO;2

Chaboureau, J.-P., & Bechtold, P. (2005). Statistical representation of clouds in a regional model and the impact on the diurnal cycle of convection during tropical convection, cirrus and nitrogen oxides (TROCCINOX). *Journal of Geophysical Research*, *110*, D17103. https://doi.org/10.1029/2004JD005645

Chaboureau, J.-P., Flamant, C., Dauhut, T., Kocha, C., Lafore, J. P., Lavaysse, C., et al. (2016). Fennec dust forecast intercomparison over the Sahara in June 2011 Atmos. *Chemical Physics*, *16*(11), 6977–6995. https://doi.org/10.5194/acp-16-6977-2016

Chaboureau, J.-P., Richard, E., Pinty, J.-P., Flamant, C., Di Girolamo, P., Kiemle, C., et al. (2011). Long-range transport of Saharan dust and its radiative impact on precipitation forecast over Western Europe: A case study during the convective and Orographically induced precipitation study (COPS). *Quarterly Journal of the Royal Meteorological Society*, *137*(S1), 236–251. https://doi.org/10.1002/qj.719

Comiso, J. C., Meier, W. N., & Gersten, R. (2017). Variability and trends in the Arctic Sea ice cover: Results from different techniques. *Journal of Geophysical Research: Oceans*, *122*, 6883–6900. https://doi.org/10.1002/2017JC012768

Comiso, J. C., Parkinson, C. L., Gersten, R., & Stock, L. (2008). Accelerated decline in the Arctic Sea ice cover. *Geophysical Research Letters*, *35*, L01703. https://doi.org/10.1029/2007GL031972

Crumeyrolle, S., Tulet, P., Gomes, L., Garcia-Carreras, L., Flamant, C., Parker, D. J., et al. (2011). Transport of dust particles from the Bodélé region to the monsoon layer - AMMA case study of the 9-14 June 2006 period. *Atmospheric Chemistry and Physics*, *11*(2), 479–494. https://doi.org/10.5194/acp-11-479-2011

Cuxart, J., Bougeault, P., & Redelsperger, J. L. (2000). A turbulence scheme allowing for mesoscale and large-eddy simulations. *Quarterly Journal of the Royal Meteorological Society*, *126*(562), 1–30. https://doi.org/10.1002/qj.49712656202

Dumont, M., Brun, E., Picard, G., Michou, M., Libois, Q., Petit, J.-R., et al. (2014). Contribution of light-absorbing impurities in snow to Greenland's darkening since 2009. *Nature Geoscience*, *7*, 509–512. https://doi.org/10.1038/NGEO2180

Egger, J., Alpert, P., Tafferner, A., & Ziv, B. (1995). Numerical experiments on the genesis of Sharav cyclones: Idealized simulations. *Tellus*, *47A*, 162–174.

Engelstaedter, S., Tegen, I., & Washington, R. (2006). North African dust emissions and transport. *Earth Science Reviews*, *79*(1-2), 73–100. https://doi.org/10.1016/j.earscirev.2006.06.004

Fiedler, S., Schepanski, K., Knippertz, P., Heinold, B., & Tegen, I. (2014). How important are atmospheric depressions and mobile cyclones for emitting mineral dust aerosol in North Africa? *Atmospheric Chemistry and Physics*, *14*(17), 8983–9000. https://doi.org/10.5194/acp-14-8983-2014

Flamant, C., Chaboureau, J. P., Parker, D. P., Taylor, C. M., Cammas, J. P., Bock, O., et al. (2007). Airborne observations of the impact of a convective system on the planetary boundary layer thermodynamics and aerosol distribution in the intertropical discontinuity region of the west African monsoon. *Quarterly Journal of the Royal Meteorological Society*, *133*(626), 1175–1189. https://doi.org/10.1002/qj.97

Flaounas, E., Kotroni, V., Lagouvardos, K., Kazadzis, S., Gkikas, A., & Hatzianastassiou, N. (2015). Cyclone contribution to dust transport over the Mediterranean region. *Atmospheric Science Letters*, *16*(4), 473–478. https://doi.org/10.1002/asl.584

Francis, J. A., & Vavrus, S. J. (2012). Evidence linking Arctic amplification toextreme weather in mid-latitudes. *Geophysical Research Letters*, *39*, L06801. https://doi.org/10.1029/2012GL051000

Franzén, L. G., Mattsson, J. O., Maartensson, U., Nihlén, T., & Rapp, A. (1994). Yellow snow over the Alps and subarctic from dust storm in Africa, march 1991. *Ambio*, 233–235.

Grini, A., Tulet, P., & Gomes, L. (2006). Dusty weather forecasts using the MesoNH mesoscale atmospheric model. *Journal of Geophysical Research*, *111*, D19205. https://doi.org/10.1029/2005JD007007

Groot Zwaaftink, C. D., Grythe, H., Skov, H., & Stohl, A. (2016). Substantial contribution of northern high-latitude sources to mineral dust in the Arctic. *Journal of Geophysical Research: Atmospheres*, *121*, 13,678–13,697. https://doi.org/10.1002/2016JD025482

Gutman, G., & Reissell, A. (Eds.). (2011). *Eurasian Arcitic Land Cover and Land Use in a Changing Climate* (306 pp.). Springer, Earth Sciences.

Hansen, J., & Nazarenko, L. (2004). Soot climate forcing via snow and ice albedos. *PNAS*, *101*, 423–428. https://doi.org/10.1073/pnas.2237157100

Hare, F. K. (1943). Atlas lee depressions and their significance for Scirocco. U.K. Meteorological Office, Synoptic Division Tech. Memo. 43, 24 pp.

Horvath, K., Fita, L., Romero, R., Ivancan-Picek, B., & Stiperski, I. (2006). Cyclogenesis in the lee of the Atlas Mountains: a factor separation numerical study. *Advances in Geosciences*, *7*, 327–331. SRef-ID: 1680–7359/adgeo/2006–7-327

Hsu, N. C., Jeong, M.-J., Bettenhausen, C., Sayer, A. M., Hansell, R., Seftor, C. S., et al. (2013). Enhanced deep blue aerosol retrieval algorithm: The second generation. *Journal of Geophysical Research: Atmospheres*, *118*, 9296–9315. https://doi.org/10.1002/jgrd.50712

IPCC (2007). Summary for Policy Makers. In *W. G. I.: Climate change 2007: The physical science basis, Contribution of Working Group I to the 4th Assessment Report of the Intergovernmental Panel on Climate Change* (chap. 7, Section 7.5, pp. 555–564). New York: Cambridge University Press.

IPCC (2014). Climate Change 2014: Synthesis Report. In Core Writing Team, R. K. Pachauri, & L. A. Meyer (Eds.), *Contribution of Working Groups I, II and III to the Fifth Assessment Report of the Intergovernmental Panel on Climate Change*, chap. 7, Section 7.3, pp. 595–605. Geneva, Switzerland: IPCC.

Knippertz, P., Deutscher, C., Kandler, K., Müller, T., Schulz, O., & Schütz, L. (2007). Dust mobilization due to density currents in the atlas region: Observations from the SAMUM 2006 field campaign. *Journal of Geophysical Research*, *112*, D21109. https://doi.org/10.1029/2007JD008774

Knippertz, P., & Fink, A. H. (2006). Synoptic and dynamic aspects of an extreme springtime Saharan dust outbreak. *Quarterly Journal of the Royal Meteorological Society*, *132*(617), 1153–1177. https://doi.org/10.1256/qj.05.109

Kylling, A., Groot Zwaaftink, C. D., & Stohl, A. (2018). Mineral dust instantaneous radiative forcing in the Arctic. *Geophysical Research Letters*, *45*, 4290–4298. https://doi.org/10.1029/2018GL077346

Lac, C., Chaboureau, J.-P., Masson, V., Pinty, J.-P., Tulet, P., Escobar, J., et al. (2018). Overview of the Meso-NH model version 5.4 and its applications. *Geoscientific Model Development*. https://doi.org/10.5194/gmd-2017-297

Lafore, J. P., Stein, J., Asencio, N., Bougeault, P., Ducrocq, V., Duron, J., et al. (1998). The Meso-NH atmospheric simulation system. Part I: Adiabatic formulation and control simulations. Scientific objectives and experimental design. *Annales de Geophysique*, *16*, 90–109.

Lambert, F., Kug, J. S., Park, R. J., Mahowald, N., Winckler, G., Abe-Ouchi, A., et al. (2013). The role of mineral-dust aerosols in polar temperature amplification. *Nature Climate Change*, *3*(5), 487–491. https://doi.org/10.1038/nclimate1785

Laurent, B., Marticorena, B., Bergametti, G., Léon, J. F., & Mahowald, N. M. (2008). Modeling mineral dust emissions from the Sahara desert using new surface properties and soil database. *Journal of Geophysical Research*, *113*, D14218. https://doi.org/10.1029/2007JD009484

Law, K. S., & Stohl, A. (2007). Arctic air pollution: Origins and impacts. *Science*, *315*(5818), 1537–1540. https://doi.org/10.1126/science.1137695

Levy, R., Hsu, C., et al., (2015). MODIS Atmosphere L2 Aerosol Product. NASA MODIS Adaptive Processing System, Goddard Space Flight Center, USA. https://doi.org/10.5067/MODIS/MYD04_L2.006

Mallet, M., Tulet, P., Serça, D., Solmon, F., Dubovik, O., Pelon, J., et al. (2009). Impact of dust aerosols on the radia-tive budget, surface heat fluxes, heating rate profiles and convec-tive activity over West Africa during March 2006. *Atmospheric Chemistry and Physics*, *9*, 7143–7160. https://doi.org/10.5194/acp-9-7143-2009

Marsham, J. H., Dixon, N. S., Garcia-Carreras, L., Lister, G., Parker, D. J., Knippertz, P., et al. (2013). The role of moist convection in the west African monsoon system: Insights from 584 continental-scale convection-permitting simulations. *Geophysical Research Letters*, *40*, 1843–1849. https://doi.org/10.1002/grl.50347

Mattingly, K. S., Mote, T. L., & Fettweis, X. (2018). Atmospheric river impacts on Greenland Ice Sheet surface mass balance. *Journal of Geophysical Research: Atmospheres*, *123*, 8538–8560. https://doi.org/10.1029/2018JD028714

McAuliffe, M. A. P., & Ruth, A. A. (2013). Typical tropospheric aerosol backscatter profiles for southern Ireland: The Cork Raman lidar. *Atmospheric Research*, 120–121.

McGuire, A. D., Chapin, F. S. III, Walsh, J. E., & Wirth, C. (2006). Integrated regional changes in arctic climate feedbacks: Implications for the global climate system. *Annual Review of Environment and Resources*, *31*(1), 61–91. https://doi.org/10.1146/annurev.energy.31.020105.100253

Meier, W. N., Hovelsrud, G. K., van Oort, B. E. H., Key, J. R., Kovacs, K. M., Michel, C., et al. (2014). Arctic Sea ice in transformation: A review of recent observed changes and impacts on biology and human activity. *Reviews of Geophysics*, *52*, 185–217. https://doi.org/10.1002/2013RG000431

Mickley, L. J., Jacob, D. J., Field, B. D., & Rind, D. (2004). Climate response to the increase in tropospheric ozone since preindustrial times: A comparison between ozone and equivalent CO2 forcings. *Journal of Geophysical Research*, *109*, D05106. https://doi.org/10.1029/2003JD003653

Mlawer, E. J., Taubman, S. J., Brown, P. D., Iacono, M. J., & CLough, S. A. (1997). Radiative transfer for inhomogeneous atmospheres: RRTM, a validated correlated-k model for the longwave. *Journal of Geophysical Research*, *102D*, 16,663–16,682.

Mote, L. T. (2007). Greenland surface melt trends 1973–2007: Evidence of a large increase in 2007. *Geophysical Research Letters*, *34*, L22507. https://doi.org/10.1029/2007GL031976

Mote, T. L., & Anderson, M. R. (1995). Variations in snowpack melt on the Greenland ice sheet based on passive-microwave measurements. *Journal of Glaciology*, *41*(137), 51–60. https://doi.org/10.1017/S0022143000017755

Papayannis, A., Amiridis, V., Mona, L., Tsaknakis, G., Balis, D., Bösenberg, J., et al. (2008). Systematic lidar observations of Saharan dust over Europe in the frame of EARLINET (2000–2002). *Journal of Geophysical Research*, *113*, D10204. https://doi.org/10.1029/2007JD009028

Pierangelo, C., Chédin, A., Heilliette, S., Jacquinet-Husson, N., & Armante, R. (2004). Dust altitude and infrared optical depth from AIRS. *Atmospheric Chemistry and Physics*, *4*(7), 1813–1822. https://doi.org/10.5194/acp-4-1813-2004

Pinty, J.-P., and Jabouille, P. (1998). A mixed-phase cloud parameterization for use in a mesoscale non-hydrostatic model: Simulations of a squall line and of orographic precipitations. Preprints, Conf. on Cloud Physics, Everett, WA, Amer. Meteor. Soc., 217–220.

Prospero, J. M., Ginoux, P., Torres, O., Nicholson, S. E., & Gill, T. E. (2002). Environmental characterization of global sources of atmospheric soil dust identified with the NIMBUS 7 Total ozone mapping spectrometer (TOMS) absorbing aerosol product. *Reviews of Geophysics*, *40*(1), 1002. https://doi.org/10.1029/2000RG000095

Qian, Y., Yasunari, T. J., Doherty, S. J., Flanner, M. G., Lau, W. K. M., Ming, J., et al. (2015). Light-absorbing particles in snow and ice: Measurement and modeling of climatic and hydrological impact. *Advances in Atmospheric Sciences*, *32*(1), 64–91.

Quinn, P. K., Bates, T. S., Baum, E., Doubleday, N., Fiore, A. M., Flanner, M., et al. (2008). Short-lived pollutants in the Arctic: Their climate impact and possible mitigation strategies. *Atmospheric Chemistry and Physics*, *8*(6), 1723–1735. https://doi.org/10.5194/acp-8-1723-2008

Quinn, P. K., Shaw, G., Andrews, E., Dutton, E. G., Ruoho-Airola, T., & Gong, S. L. (2007). Arctic haze: Current trends and knowledge gaps. *Tellus B*, *59*(1), 115–129. https://doi.org/10.1111/j.1600-0889.2006.00238.x

Richter-Menge, J., Jeffries, M. O., & Osborne, E. (Eds.) (2018). The Arctic [in "State of the Climate in 2017"]. *Bulletin of the American Meteorological Society*, *99*(8), S143–173. https://doi.org/10.1175/2018BAMSStateoftheClimate.1

Rodríguez, E., Toledano, C., Cachorro, V. E., Ortiz, P., Stebel, K., Berjón, A., et al. (2012). Aerosol characterization at the sub-Arctic site Andenes (69°N, 16°E), by the analysis of columnar optical properties. *Quarterly Journal of the Royal Meteorological Society*, *138*(663), 471–482. https://doi.org/10.1002/qj.921

Ryan, C. J., Hubbard, A., Stibal, M., Irvine-Fynn, T. D., Cook, J., Smith, L. C., et al. (2018). Dark zone of the Greenland ice sheet controlled by distributed biologically-active impurities. *Nature Communications*, *9*, 1065. https://doi.org/10.1038/s41467-018-03353-2

Schepanski, K., Tegen, I., Laurent, B., Heinold, B., & Macke, A. (2007). A new Saharan dust source activation frequency map derived from MSG-SEVIRI IR channels. *Geophysical Research Letters*, *34*, L18803. https://doi.org/10.1029/2007GL030168

Schepanski, K., Tegen, I., & Macke, A. (2012). Comparison of satellite based observations of Saharan dust source areas. *Remote Sensing of Environment*, *123*, 90–97. https://doi.org/10.1016/j.rse.2012.03.019

Schepanski, K., Tegen, I., Todd, M. C., Heinold, B., Bönisch, G., Laurent, B., et al. (2009). Meteorological processes forcing Saharan dust emission inferred from MSG-SEVIRI observations of sub-daily dust source activation. *Journal of Geophysical Research*, *114*, D10201. https://doi.org/10.1029/2008JD010325

Serreze, M. C., & Francis, J. A. (2006). The Arctic Amplification Debate. *Climatic Change*, *76*(3–4), 241.

Shindell, D., & Faluvegi, G. (2009). Climate response to regional radiative forcing during the twentieth century. *Nature Geoscience*, *2*(4), 294–300. https://doi.org/10.1038/ngeo473

Shindell, D. T., Faluvegi, G., Bauer, S. E., Koch, D. M., Unger, N., Menon, S., et al. (2007). Climate response to projected changes in short-lived species under an A1B scenario from 2000–2050 in the GISS climate model. *Journal of Geophysical Research*, *112*, D20103. https://doi.org/10.1029/2007JD008753

Stohl, A. (2006). Characteristics of atmospheric transport into the Arctic troposphere. *Journal of Geophysical Research*, *111*, D11306. https://doi.org/10.1029/2005JD006888

Stroeve, J. C., Markus, T., & Meier, W. N. (2006). Recent changes in the Arctic melt season. *Annals of Glaciology*, *44*, 367–374. https://doi.org/10.3189/172756406781811583

Stroeve, J. C., Mioduszewski, J. R., Rennermalm, A., Boisvert, L. N., Tedesco, M., & Robinson, D. (2017). Investigating the Local Scale Influence of Sea Ice on Greenland Surface Melt. *The Cryosphere Discussions*, *11*, 1–36. https://doi.org/10.5194/tc-2017-65

Sutton, L. J. (1925). Haboobs. *Quarterly Journal of the Royal Meteorological Society*, *51*, 25–30.

Sutton, L. J. (1931). Haboobs. *Quarterly Journal of the Royal Meteorological Society*, *57*, 143–161.

Tedesco, M., Box, J. E., Cappelen, J., Fettweis, X., Mote, T., Rennermalm, A. K., et al. (2014). Greenland Ice Sheet in [2013 NOAA Arctic Report Card], NOAA.

Tedesco, M., Doherty, S., Warren, W., Tranter, M., Stroeve, J., Fettweis, X., et al. (2015). What darkens the Greenland ice sheet? *Eos*, *96*. https://doi.org/10.1029/2015EO035773

Thorncroft, C. D., & Flocas, H. A. (1997). A case study of Saharan cyclogenesis. *Monthly Weather Review*, *125*(6), 1147–1165. https://doi.org/10.1175/1520-0493(1997)125<1147:ACSOSC>2.0.CO;2

Todd, M. C., Bou Karam, D., Cavazos, C., Bouet, C., Heinold, B., Baldasano, J. M., et al. (2008). Quantifying uncertainty in estimates of mineral dust flux: An inter-comparison of model performance over the Bodélé depression, northern Chad. *Journal of Geophysical Research*, *113*, D24107. https://doi.org/10.1029/2008JD010476

Todd, M. C., Washington, R., Raghavan, S., Lizcano, G., & Knippertz, P. (2008). Regional model simulations of the Bodélé low-level jet of northern Chad during the Bodélé dust experiment (BoDEx 2005). *Journal of Climate*, *21*(5), 995–1012. https://doi.org/10.1175/2007JCLI1766.1

Trigo, I. F., Bigg, G. R., & Davies, T. D. (2002). Climatology of cyclogenesis mechanisms in the Mediterranean. *Monthly Weather Review*, *130*(3), 549–569. https://doi.org/10.1175/1520-0493(2002)130<0549:COCMIT>2.0.CO;2

Tulet, P., Crassier, V., Cousin, F., Shure, K., & Rosset, R. (2005). ORILAM, A three moment lognormal aerosol scheme for mesoscale atmospheric model. On-line coupling into the Meso-NH-C model and validation on the Escompte campaign. *Journal of Geophysical Research*, *110*, D18201. https://doi.org/10.1029/2004JD005716

Tulet, P., Mallet, M., Pont, V., Pelon, J., & Boone, A. (2008). The 7–13 March 2006 dust storm over West Africa: Generation, transport, and vertical stratification. *Journal of Geophysical Research*, *113*, D00C08. https://doi.org/10.1029/2008JD009871

VanCuren, R. A., Cahill, T., Burkhart, J., Barnes, D., Zhao, Y., Perry, K., et al. (2012). Aerosols and their sources at summit Greenland—First results of continuous size- and time-resolved sampling. *Atmospheric Environment*, *52*, 82–97. https://doi.org/10.1016/j.atmosenv.2011.10.047

Washington, R., & Todd, M. C. (2005). Atmospheric controls on mineral dust emission from the Bodélé depression, Chad: The role of the low level jet. *Geophysical Research Letters*, *32*, L17701. https://doi.org/10.1029/2005GL023597

Westphal, D. L., Toon, O. B. and Carlson, T. N. (1985). A Numerical investigation of Saharan Dust Storms, Ph. D. Thesis, Penn. State Univ., University Park.

Williams, E. R., Nathou, N., Hicks, E., Pontikis, C., Russell, B., Miller, M., et al. (2009). The electrification of dust-lofting gust fronts ('haboobs') in the Sahel. *Atmospheric Research*, *91*(2-4), 292–298. https://doi.org/10.1016/j.atmosres.2008.05.017

Zender, C. S., Bian, H. S., & Newman, D. (2003). Mineral dust entrainment and deposition (DEAD) model: Description and 1990s dust climatology. *Journal of Geophysical Research*, *108*(D14), 4416. https://doi.org/10.1029/2002JD002775